Electronic Supplementary Material (ESI) for Polymer Chemistry.

Supporting information

Sphere-to-worm morphological transitions and size changes through thiol–*para*-fluoro core modification of PISA-made nano-objects

Nicolas Busatto,[a] Joseph L. Keddie,[b] Peter J. Roth[a,]*

[a] Department of Chemistry, University of Surrey, Guildford, Surrey, GU2 7XH, UK

[b] Department of Physics, University of Surrey, Guildford, Surrey, GU2 7XH, UK

Contents

1. Materials

All reagents and solvents were purchased from Sigma-Aldrich or Fisher Scientific and used as received unless stated otherwise. All monomers were passed through a column of basic aluminium oxide to remove inhibitors prior to use. 2,2-Azobisisobutyronitrile (AIBN) was recrystallized from methanol. 2,3,4,5,6-Pentafluorobenzyl methacrylate (PFBMA) was prepared as described elsewhere.[1]

2. Instrumentation

Nuclear magnetic resonance (NMR) spectroscopy: ^{1}H, ^{13}C and ^{19}F NMR spectra were recorded on a 400 MHz or 500 MHz Bruker spectrometer in deuterated chloroform ($CDCl_3$, δ = 7.26 ppm). Samples were prepared in 5 mm NMR tubes in which 50–100 µL of solution (*i.e.* crude reaction mixture or dispersed samples) or 5–30 mg of dried product was dissolved in $CDCl_3$ to a total volume of 400–500 µL.

Size exclusion chromatography (SEC) was performed on a Viscotek GPCMax VE 2001 setup with three linear 7.5×300 mm PLgel mixed-D columns connected to a Viscotek VE3580 refractive index (RI) detector and a Malvern 270 dual detector (viscometer and light scattering). The instrument operated at 35 °C with tetrahydrofuran (THF) containing 250 ppm BHT as mobile phase at a flow rate of 1.0 mL×min^{-1}. The system was calibrated using a series of narrow molecular weight distribution PMMA standards with molecular weights ranging from 5 kg×mol^{-1} to 298 kg×mol^{-1} and reported values are PMMA equivalent molar masses. Samples were prepared by dissolving dried polymers in the mobile phase targeting a concentration of 1–4 g×L^{-1}. After letting samples dissolve for 24 h, they were filtered (0.2 µm regenerated cellulose syringe filter) prior to injection.

Dynamic Light Scattering (DLS) was performed on a Malvern Zetasizer Nanoseries instrument in glass cuvettes. Samples were prepared by dilution of dispersions in the dispersant (ethanol) at a concentration near 1 g×L^{-1}. Samples were not filtered. Reported values are averages from five individual measurements.

Scanning Transmission Electron Microscopy (STEM) images were recorded on a Hitachi HD-2700 operating at a maximum accelerating voltage of 200 kV or Jeol JEM1010 operating at a maximum accelerating voltage of 80 kV. A drop of diluted solution of PISA particles was placed on a carbon-coated copper grid (300 mesh Cu grid, Agar Scientific). Excess PISA solution was wicked away from the grid with filter paper. A drop of lead acetate (0.2 wt% in ethanol) was added on top to stain the particles. Excess staining solution was wicked away from the grid with filter paper. Samples were prepared at room temperature.

Number-average particle diameters (D_{Num}), volume-average particle diameters (D_{Vol}), and diameter dispersities ($Đ$) were calculated by measuring at least 100 particles using ImageJ software and using the following equations: $D_{Num} = \frac{\sum n_i d_i}{\sum n_i}$, $D_{Vol} = \frac{\sum n_i {d_i}^4}{\sum n_i {d_i}^3}$ and $Đ = \frac{D_{Vol}}{D_{Num}}$, where n_i is the number of particles of diameter d_i, as measured manually with the measuring tool in ImageJ software. At least 100 particles were randomly chosen and used to calculate the diameters.

Differential scanning calorimetry (DSC) was performed on a DSC Q1000 (TA Instruments) in aluminum pans with a second aluminum pan as a reference sample. The glass transition temperature, T_g, was determined from the second heating step of a heat–cool–heat cycle (−50 °C to 210 °C at 10 °C/min) from the intersection of the two tangents drawn on the heat flow curve before the onset and at the inflection point of the relaxation process (drop of heat flow).

The tangents were automatically placed by the software (TA Universal Analysis) after manually defining the limits (start and end) of the relaxation process.

Contact Angle Measurements. Thin polymer films were deposited on (100) silicon wafers (approximately 4 cm^2) by spin coating 5 wt-% polymer solutions in THF. Two drops of solution were spun for 30 sec at 2000 rpm. The deposited films were allowed to dry at room temperature for 3 days. Contact angles were measured with a drop shape analyser DSA25 (Kruss) on a sessile drop of ethanol (96%) dispensed manually (5µL). A video was recorded by the built-in camera which was focused on the needle of the syringe prior to the experiment. Kruss Advance software was used to automatically determine the contact angles. The reported value is an average of six measurements which ranged from 14° to 18°.

3. Synthesis and characterisations

3.1.Poly[poly(ethylene glycol) methyl ether methacrylate] (pPEGMA) macro-CTAs

pPEGMAs (monomer molecular weight = 480 g/mol) were synthesised in ethanol (96%) and purified by dialysis and freeze drying as described previously.[2] ^{1}H NMR (500 MHz, $CDCl_3$), δ/ppm: 4.08 (s, 2 H, COOCH_2), 3.65 (m, 12–16 H, OCH_2), 3.55 (m, 2 H, CH_2OCH$_3$), 3.37 (s, 3 H, OCH_3), 2.06–1.68 (m, 2 H, CH_2 backbone), 1.1–0.77 (m, 3 H, CH_3 backbone). FT-IR, ν/cm^{-1} = 2871 (w, sp^3 C–H stretch), 1726 (s, ester C=O stretch), 1101 (s, ether and ester C–O stretch).

Table S1: Details of synthesis of $pPEGMA_x$ macro RAFT agents

Entry	Macro-CTA	Target DP	Conversion [a]	Reaction Time	$M_n^{MNR\ a}$	M_n^{SEC}	$Đ^{SEC}$
			%	h	kg/mol	kg/mol	
1	$pPEGMA_{15}$	20	74	7	4.8	4.8	1.16
2	$pPEGMA_{16}$	20	78	7	5.1	4.8	1.21
3	$pPEGMA_{28}$	30	93	17	8.7	6.9	1.18

[a]As determined by ^{1}H NMR before purification.

3.2.pPEGMA-pPFBMA nanoparticles

PPEGMA-pPFBMA nanoparticles were synthesised with a total solid content of 20 wt-% as described by Busatto *et al.*[2] ^{1}H NMR (400 MHz, $CDCl_3$), δ/ppm: 5.04 (COOCH_2, PFBMA), 4.08 (COOCH_2, PEGMA), 3.66–3.61 (m, OCH_2, PEGMA), 3.57–3.53 (CH_2OCH$_3$), 3.38 (OCH_3), 2.02–1.57 (m, CH_2 backbone), 1.14–0.67 (m, CH_3 backbone). ^{19}F NMR (376 MHz, $CDCl_3$), δ/ppm: −141.9 (5%), −142.1 (35%), and −142.4 (60%) (3 m, 2 F, *ortho*); −151.9 (58%), −152.4 (37%), and −152.8 (5%) (3 m, 1 F, *para*); −161.5 (60%), −161.8 (35%), and −162.1 (5%) (3 m, 2 F, *meta*). PFBMA degrees of polymerization, y, were calculated through comparison of the integrals of the ^{1}H NMR signals of the respective side chain COOCH_2 signals.

Table S2. Details of diblock copolymer nanoparticles

Diblock Copolymer	M_n^{MNR} kg/mol	M_n^{SEC} kg/mol	$Đ^{SEC}$	D_h^{DLS} nm	PDI^{DLS}	Morph.[a]
$pPEGMA_{16}$-$pPFBMA_{67}$	23.0	16.3	1.40	174	0.56	W[b]
$pPEGMA_{15}$-$pPFBMA_{59}$	20.5	13.9	1.43	52	0.12	S
$pPEGMA_{28}$-$pPFBMA_{48}$	21.4	14.7	1.40	27	0.11	S
$pPEGMA_{28}$-$pPFBMA_{56}$	23.5	15.2	1.49	31	0.07	S
$pPEGMA_{28}$-$pPFBMA_{70}$	27.3	16.2	1.48	38	0.05	S
$pPEGMA_{30}$-$pPFBMA_{195}$	61.1	42.0	1.40	61	0.08	-

[a] Morphology determined by STEM imaging at 25 °C

[b] This sample was found to undergo a reversible degelation from gel (5 °C) to liquid (60 °C).

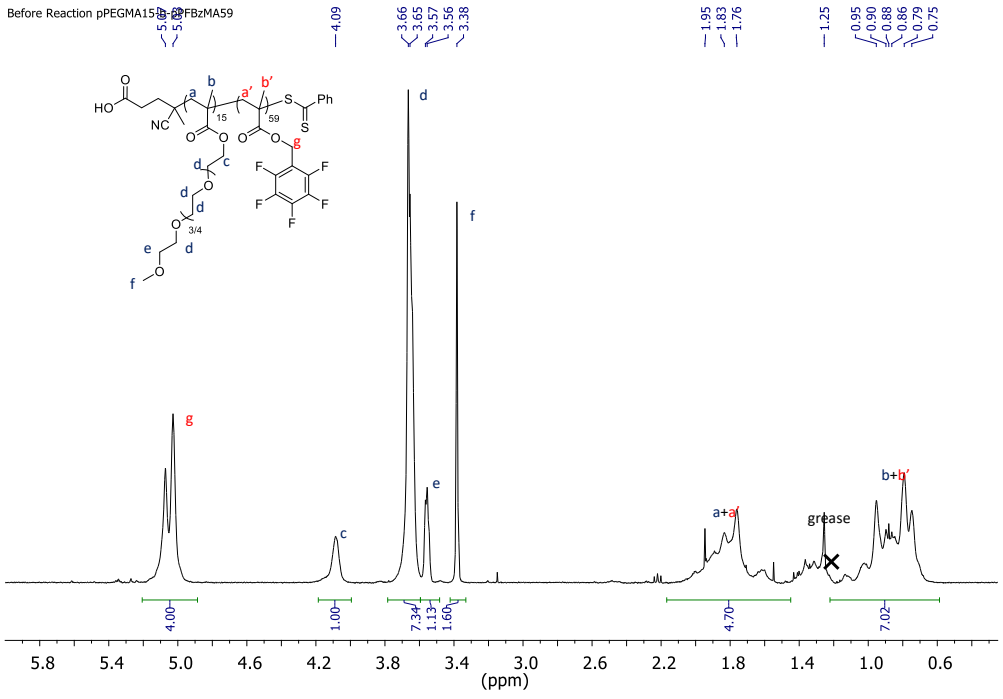

Figure S1. Exemplary ^{1}H NMR spectrum of $pPEGMA_{15}$-$pPFBMA_{59}$

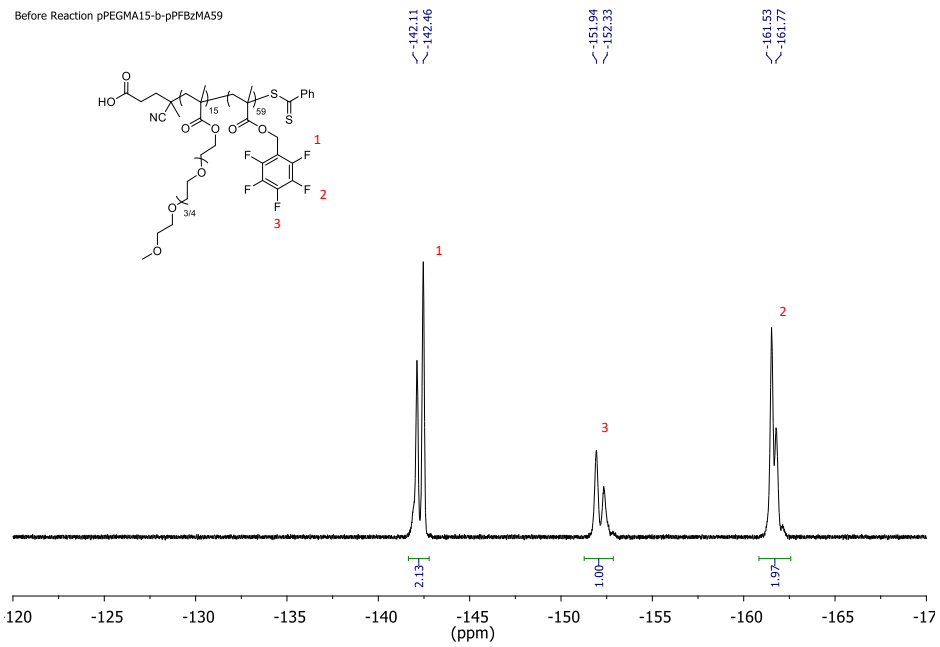

Figure S2. Exemplary ^{19}F NMR spectrum of pPEGMA$_{15}$-pPFBMA$_{59}$. Splitting of signals is due to tacticity.

Kinetics of the reaction

The kinetics data of the RAFT dispersion polymerisation of PFBMA mediated by pPEGMA$_{30}$ targeting a DP of 200 was also obtained. The PFBMA conversion reached a near-quantitative plateau within 8 hours (plot A, Figure S3). This is relatively slow but when compared to its hydrogen (non-fluorinated) analogue (benzyl methacrylate) it is in agreement with the literature that reported similar polymerisation kinetics in ethanol[3,4] or in mineral oil.[5] The rate of the RAFT polymerisation has a first-order kinetic behaviour due to negligible radical termination reactions and a constant concentration of propagating chains (pseudo first-order). The main feature of a first order polymerisation is that $\ln([M]_0/[M])$ is a linear function of time. However, the semilogarithmic plot (plot B, Figure S3) does not show a linear dependence of $\ln([M]_0/[M])$ with time. It shows that in the first 3 hours the rate of polymerisation (linear) is slower that in the next five hours (still linear) and thus that the polymerisation proceeds much faster as the concentration of monomer decreases. This phenomenon was encountered multiples times in

RAFT dispersion polymerisation and was explained by Blanazs et al.[6] to be due to the unreacted monomer that migrates into the cores of the particles and creates a relatively high local monomer concentration in the core (where the polymerisation occurs). After 3 hours, the first-order is observed up to 90% conversion. Molecular weights for each aliquot were determined by SEC (and expressed as pMMA equivalents) and data points show a linear evolution of the number-average molecular weight Mn^{SEC} with conversion (plot C, Figure S3). They also show relatively constant and narrow molecular weight distributions (D, Figure S3). Both are characteristic of RAFT polymerisation, and thus confirm that RAFT can successfully control the dispersion polymerisation of PFBMA in ethanol.

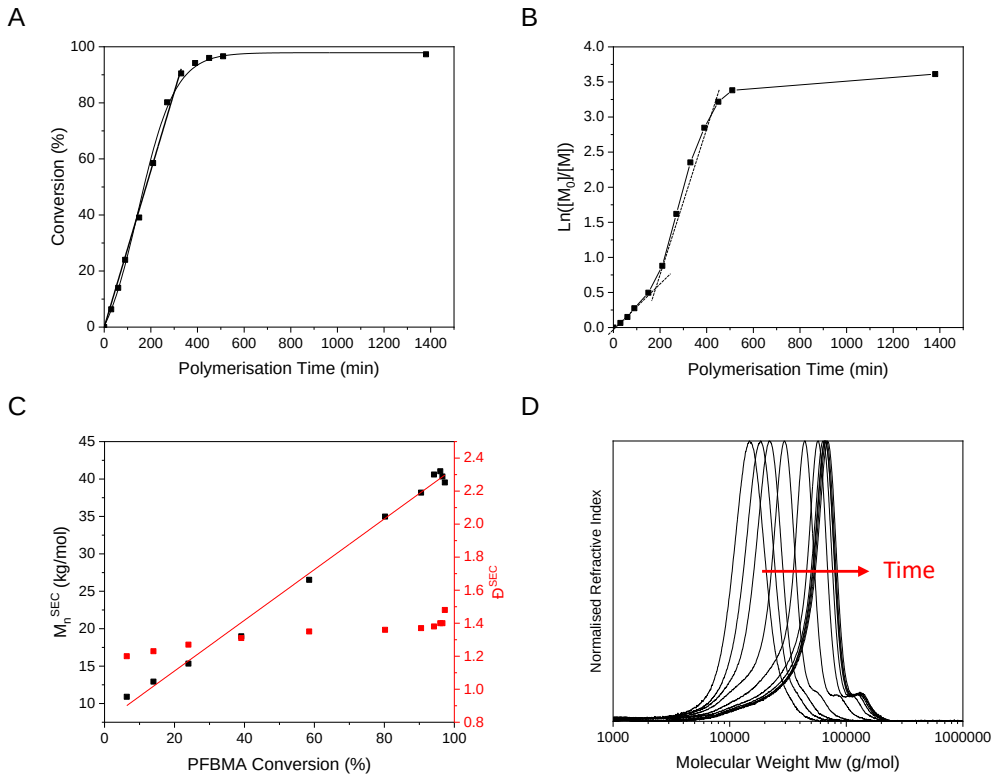

Figure S3. Kinetic plots of the RAFT dispersion polymerisation of PFBMA using $pPEGMA_{30}$ in ethanol at 70 °C. (A) Conversion vs. time; (B) Semilogarithmic plots vs. time. (C) Molecular weight M_n determined by SEC and associated dispersity vs. conversion; (D) THF SEC chromatograms.

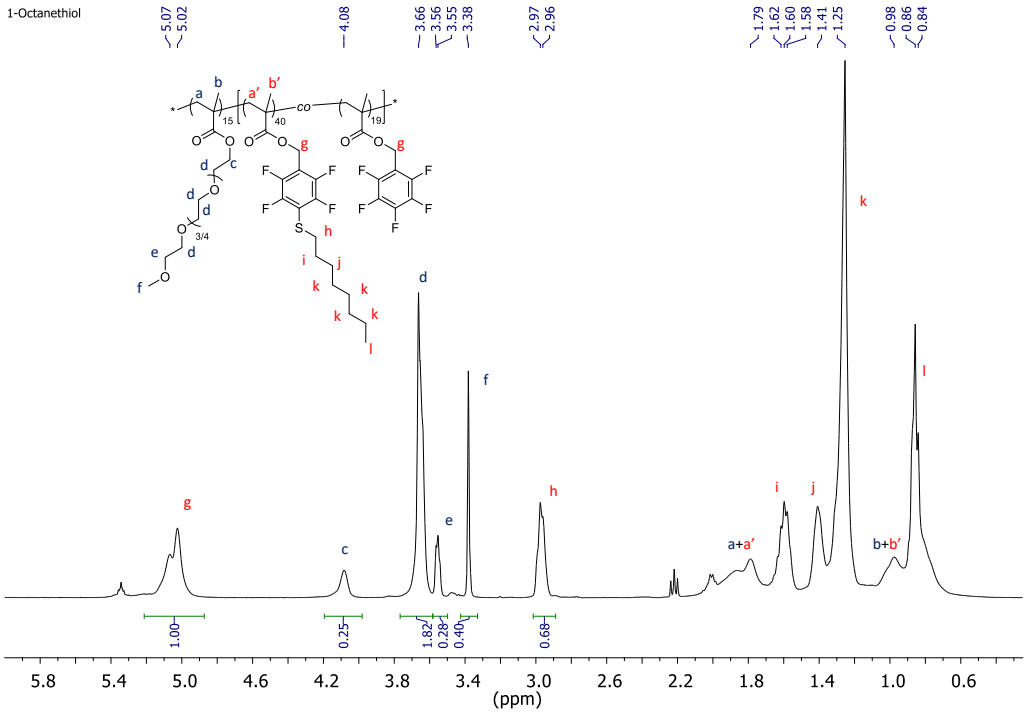

Figure S4. ^{1}H NMR spectrum of pPEGMA$_{15}$-pPFBMA$_{59}$ modified by 1-octanethiol (68% conversion)

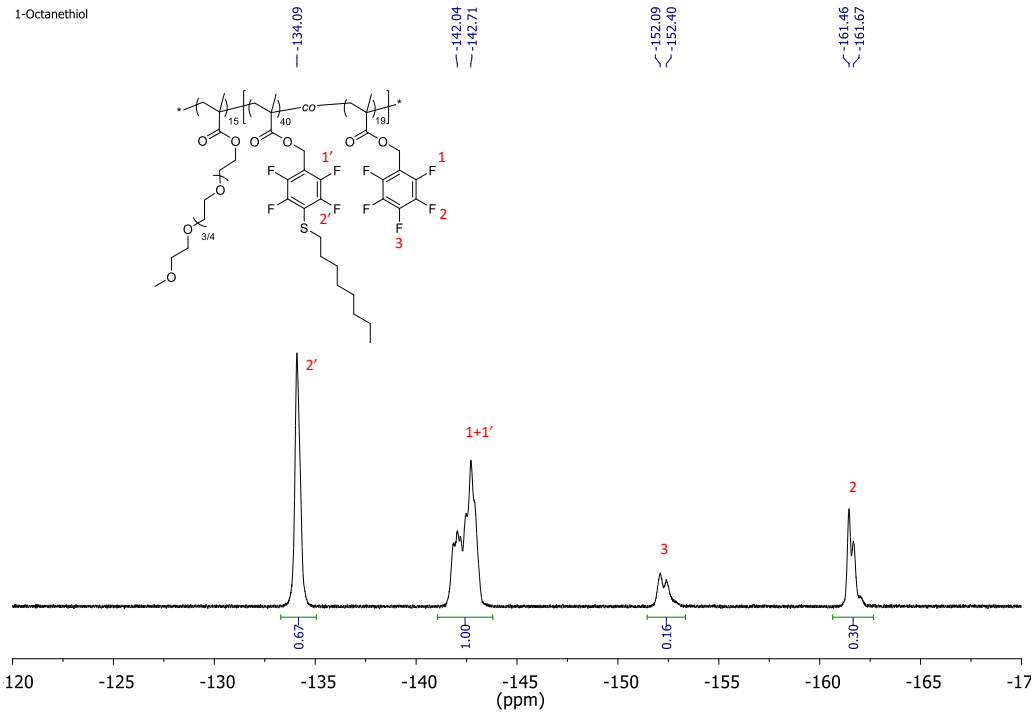

Figure S5. ^{19}F NMR spectrum of pPEGMA$_{15}$-pPFBMA$_{59}$ modified by 1-octanethiol (68% conversion)

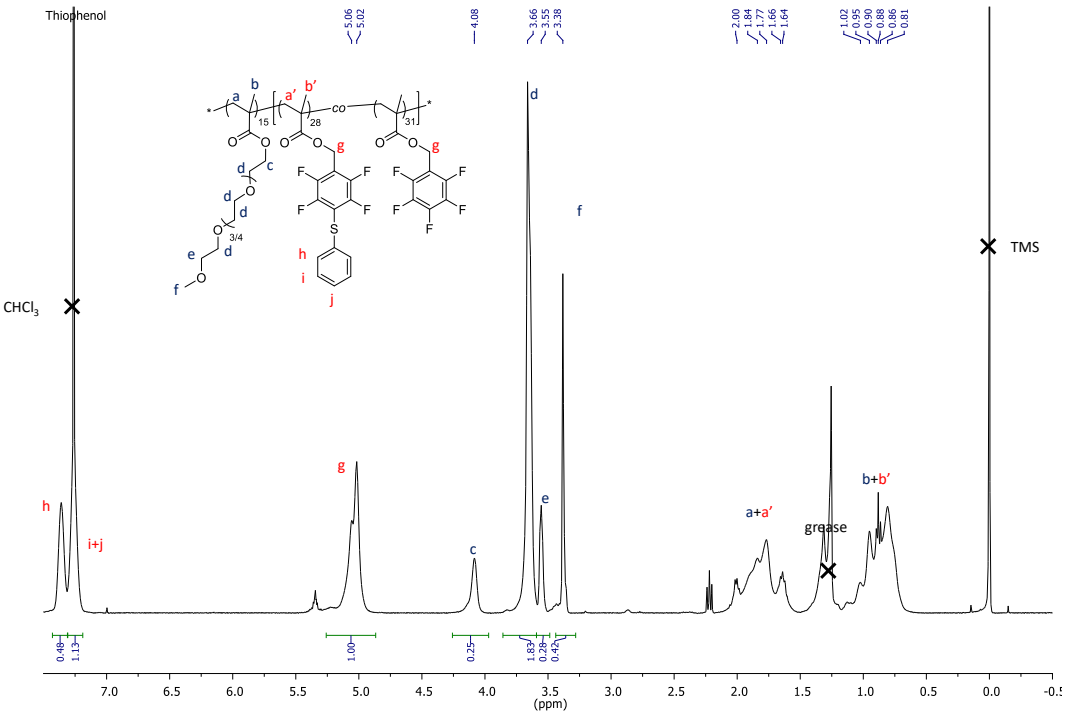

Figure S6. ^{1}H NMR spectrum of pPEGMA$_{15}$-pPFBMA$_{59}$ modified by benzenethiol (48% conversion)

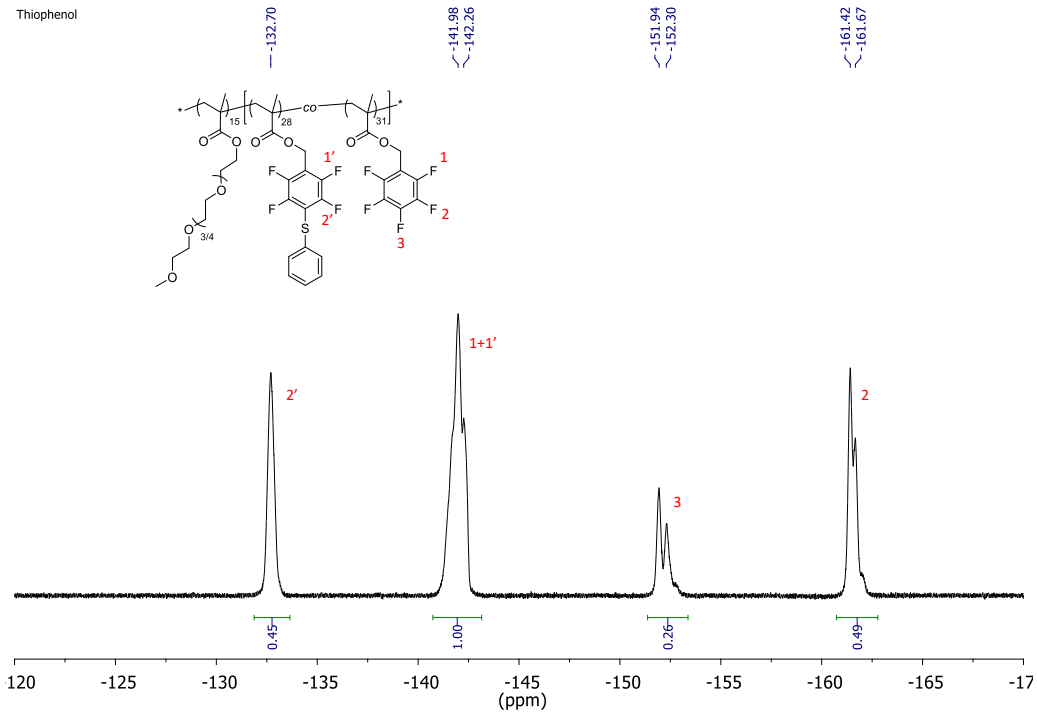

Figure S7. ^{19}F NMR spectrum of pPEGMA$_{15}$-pPFBMA$_{59}$ modified by benzenethiol (48% conversion)

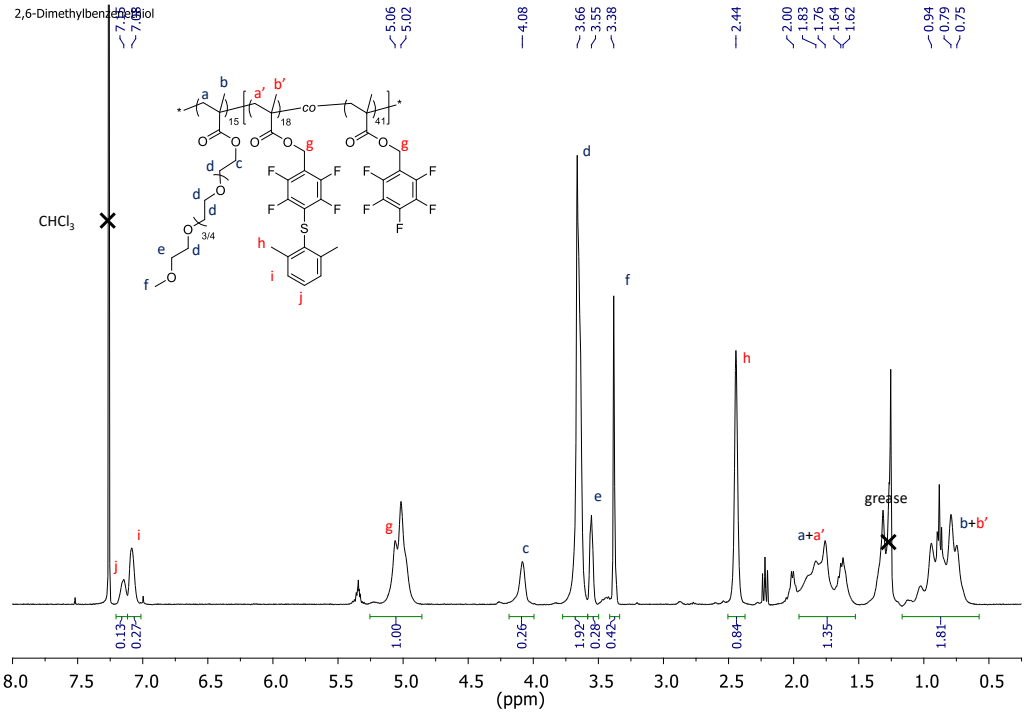

Figure S8. ^{1}H NMR spectrum of pPEGMA$_{15}$-pPFBMA$_{59}$ modified by 2,6-dimethylbenzenethiol (30% conversion)

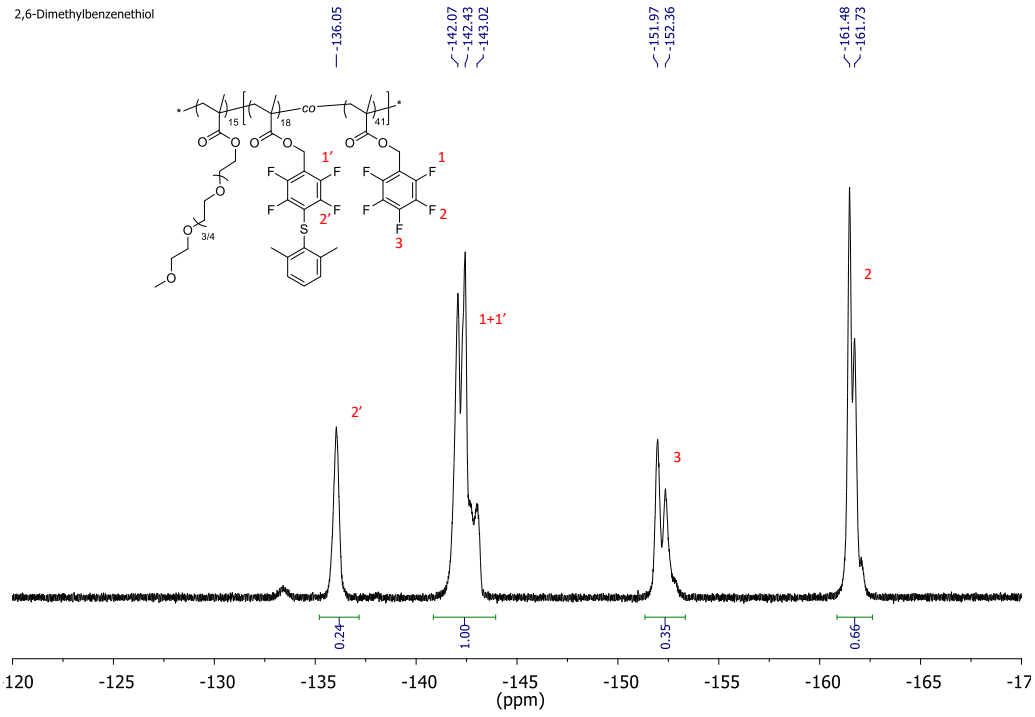

Figure S9. ^{19}F NMR spectrum of pPEGMA$_{15}$-pPFBMA$_{59}$ modified by 2,6-dimethylbenzenethiol (30% conversion).

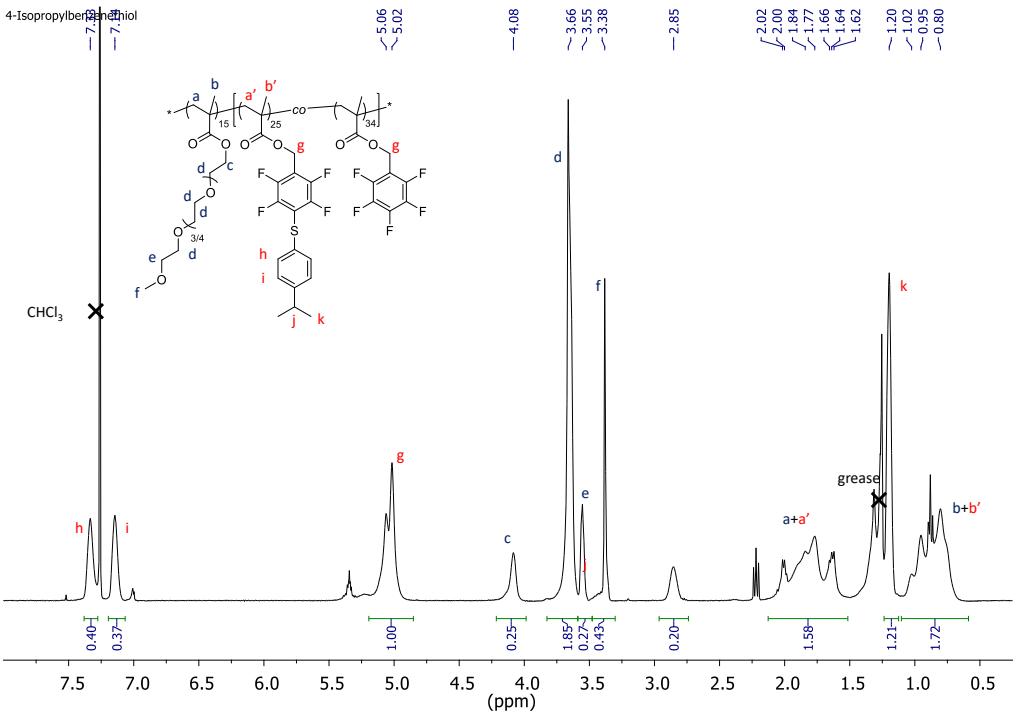

Figure S10. *^{1}H NMR spectrum of pPEGMA$_{15}$-pPFBMA$_{59}$* modified by 4-isopropylbenzenethiol (42% conversion)

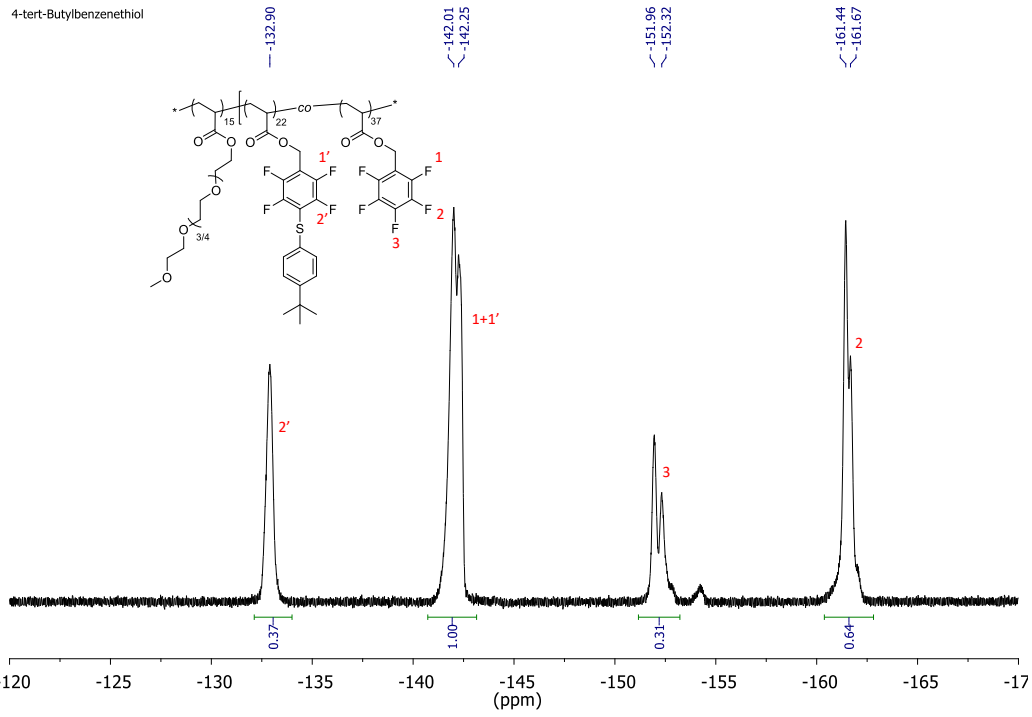

Figure S11. ^{19}F NMR spectrum of pPEGMA$_{15}$-pPFBMA$_{59}$ modified by 4-isopropylbenzenethiol (42% conversion)

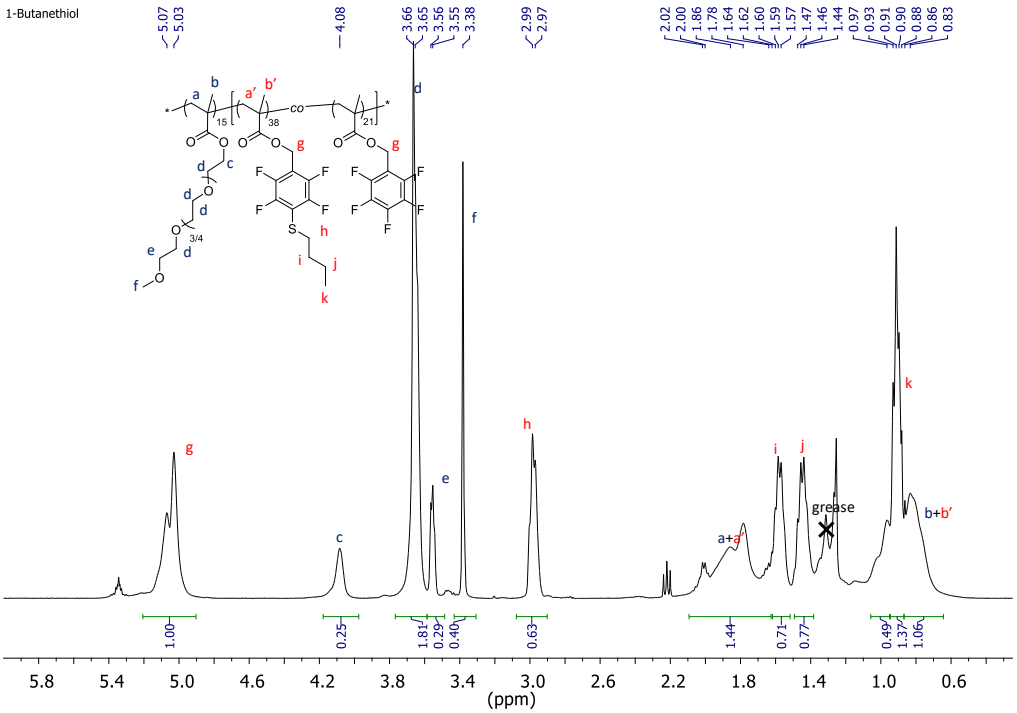

Figure S12. ^{1}H NMR spectrum of pPEGMA$_{15}$-pPFBMA$_{59}$ modified by 1-butanethiol (64% conversion)

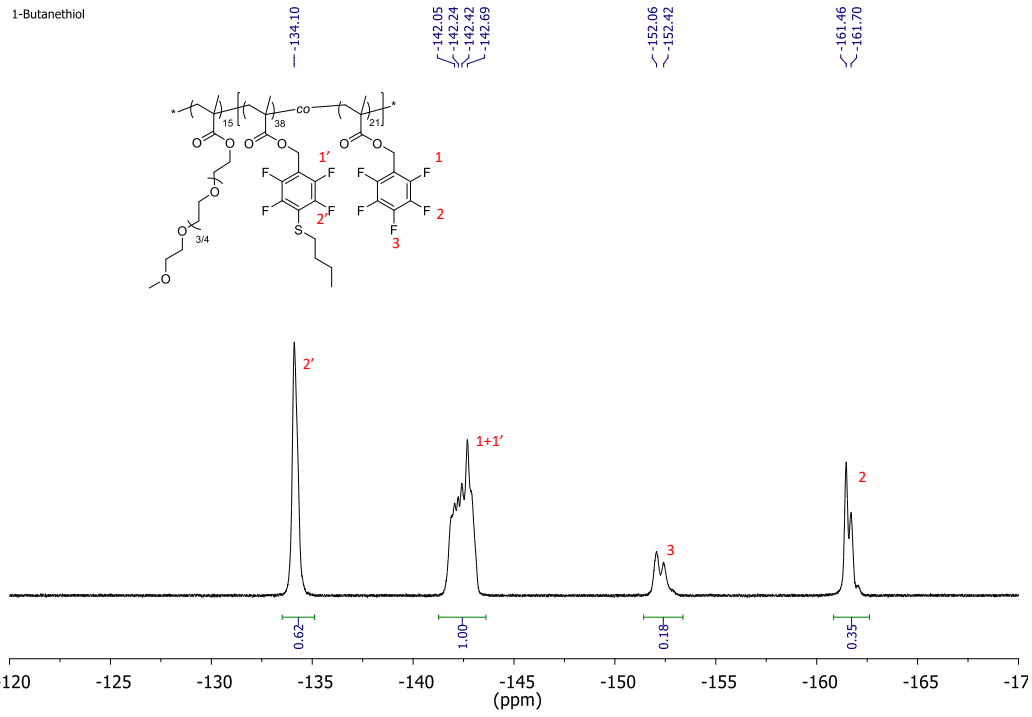

Figure S13. ^{19}F NMR spectrum of pPEGMA$_{15}$-pPFBMA$_{59}$ modified by 1-butanethiol (64% conversion).

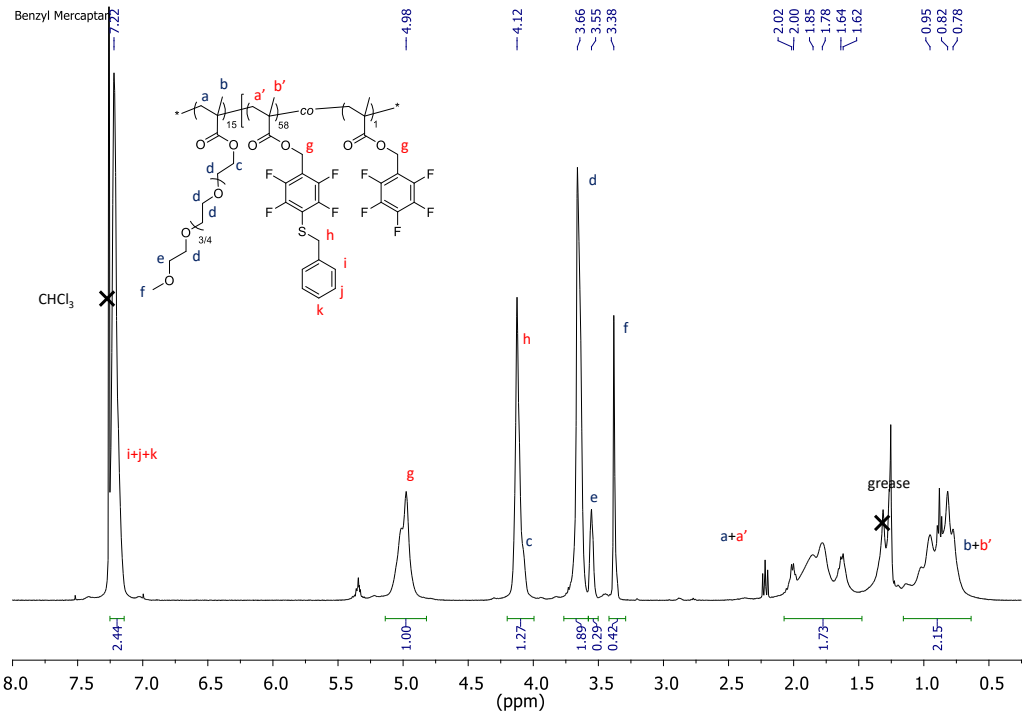

Figure S14. ^{1}H NMR spectrum of pPEGMA$_{15}$-pPFBMA$_{59}$ modified by benzyl mercaptan (98% conversion)

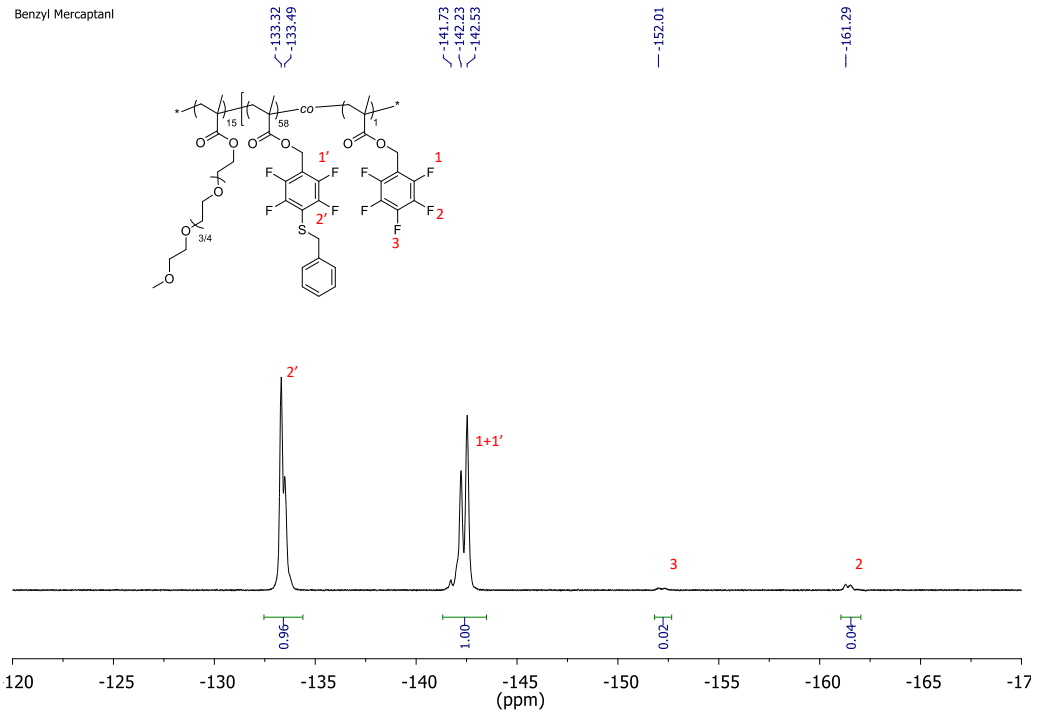

Figure S15. ^{19}F NMR spectrum of pPEGMA$_{15}$-pPFBMA$_{59}$ modified by benzyl mercaptan (98% conversion).

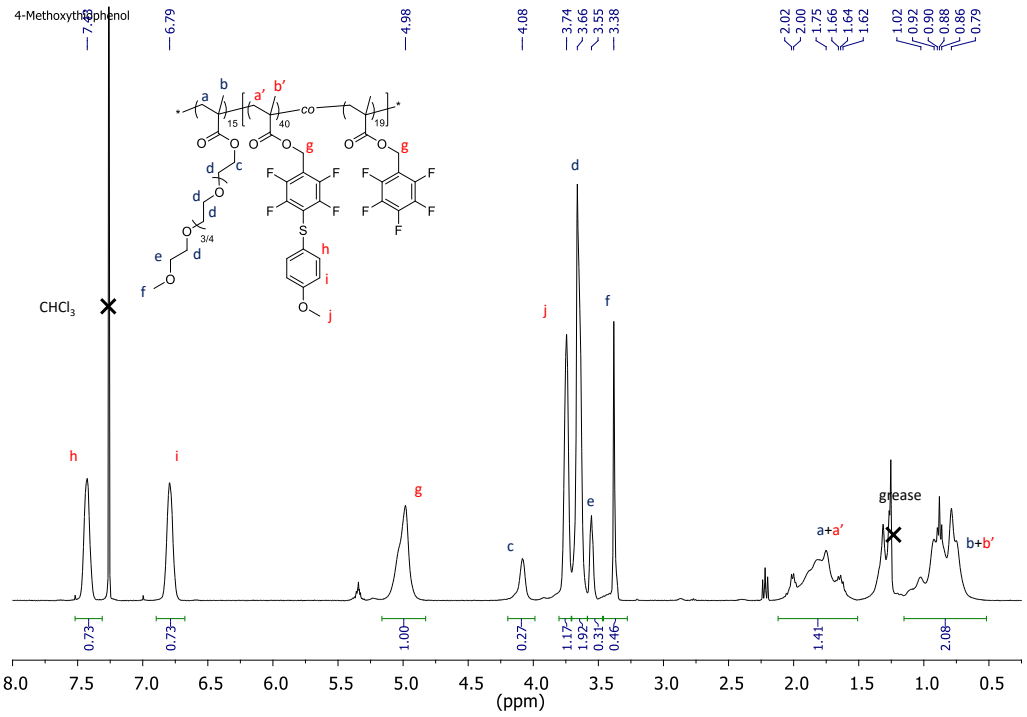

Figure S16. ^{1}H NMR spectrum of pPEGMA$_{15}$-pPFBMA$_{59}$ modified by 4-methoxybenzenethiol (68% conversion)

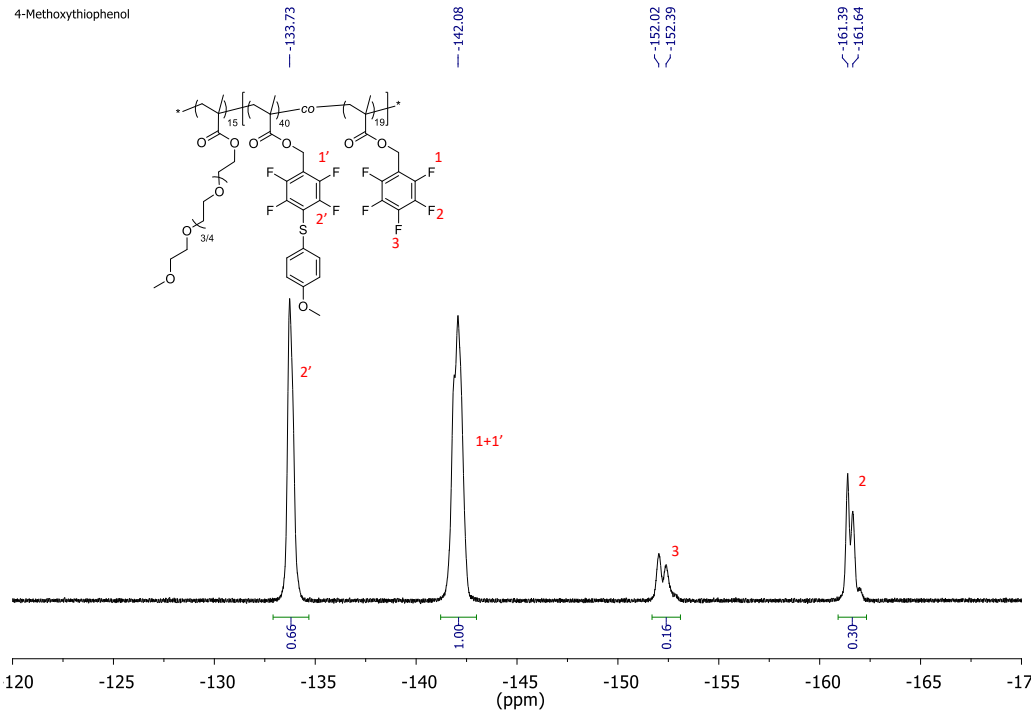

Figure S17. ^{19}F NMR spectrum of pPEGMA$_{15}$-pPFBMA$_{59}$ modified by 4-methoxybenzenethiol (68% conversion).

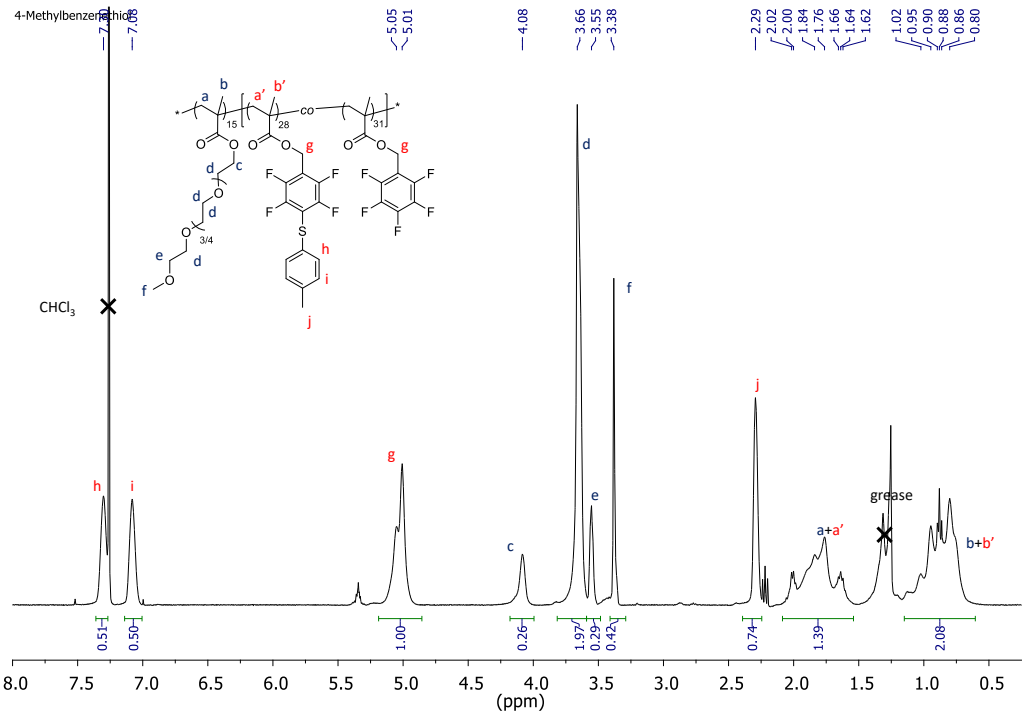

Figure S18. ^{1}H NMR spectrum of pPEGMA$_{15}$-pPFBMA$_{59}$ modified by 4-methylbenzenethiol (48% conversion)

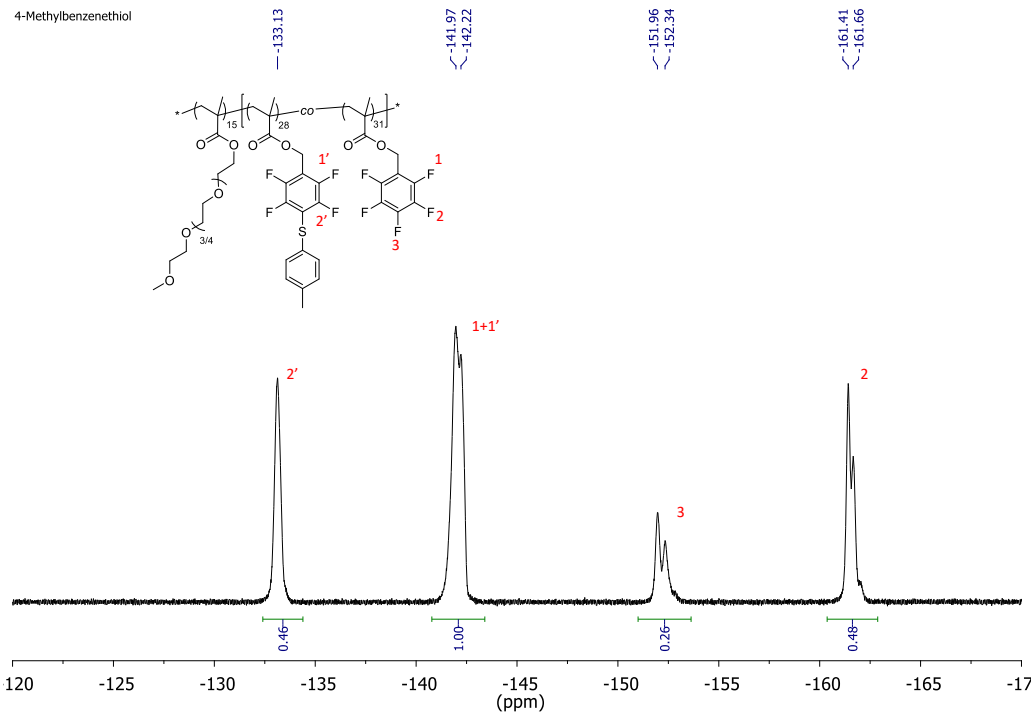

Figure S19. ^{19}F NMR spectrum of pPEGMA$_{15}$-pPFBMA$_{59}$ modified by 4-methylbenzenethiol (48% conversion).

3.3. Gelation of a worm sample

Figure S20. Photograph of a vial standing upside-down and containing a gel formed by reaction of a (liquid) pPEGMA$_{15}$-pPFBMA$_{59}$ sphere dispersion with 1-butanethiol (table 1, entry 22 in main text). After modification and purification by dialysis, the dispersion was concentrated by evaporation to a solid content of approx. 20 wt%.

Table S3 Characterisation of thiol-modified pPFBMA$_{70}$ homopolymers

Entry	Homopolymer pPFBMA$_{70}$ modified by thiol	Para-fluoro Conversion (%)[a]	T_g (°C)[b]	Heat Capacity Change, ΔC_p (J/K)[b]
1	pTFBMA-Butanethiol	100	13.4	0.00169
2	pTFBMA-Benzyl mercaptan	100	50.6	0.00138
3	pTFBMA-4-Isopropylbenzenethiol	100	68.1	0.00110
4	pTFBMA-Benzenethiol	95	70.9	0.00134
5	pTFBMA-4-tert-Butylbenzenethiol	96	90.7	0.00117

[a] as measured by ^{19}F NMR; [b] as determined by DSC

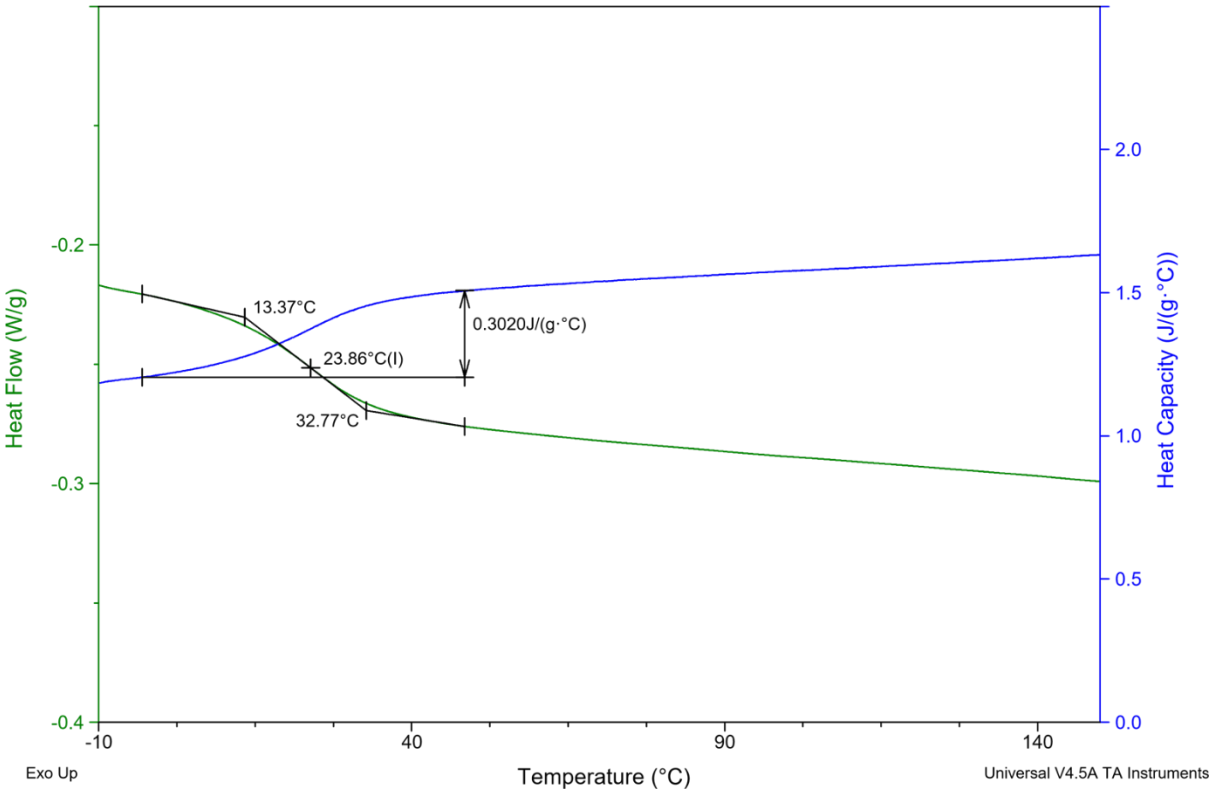

Figure S21. DSC traces of pTFBMA-Butanethiol (Table S3, entry 1)

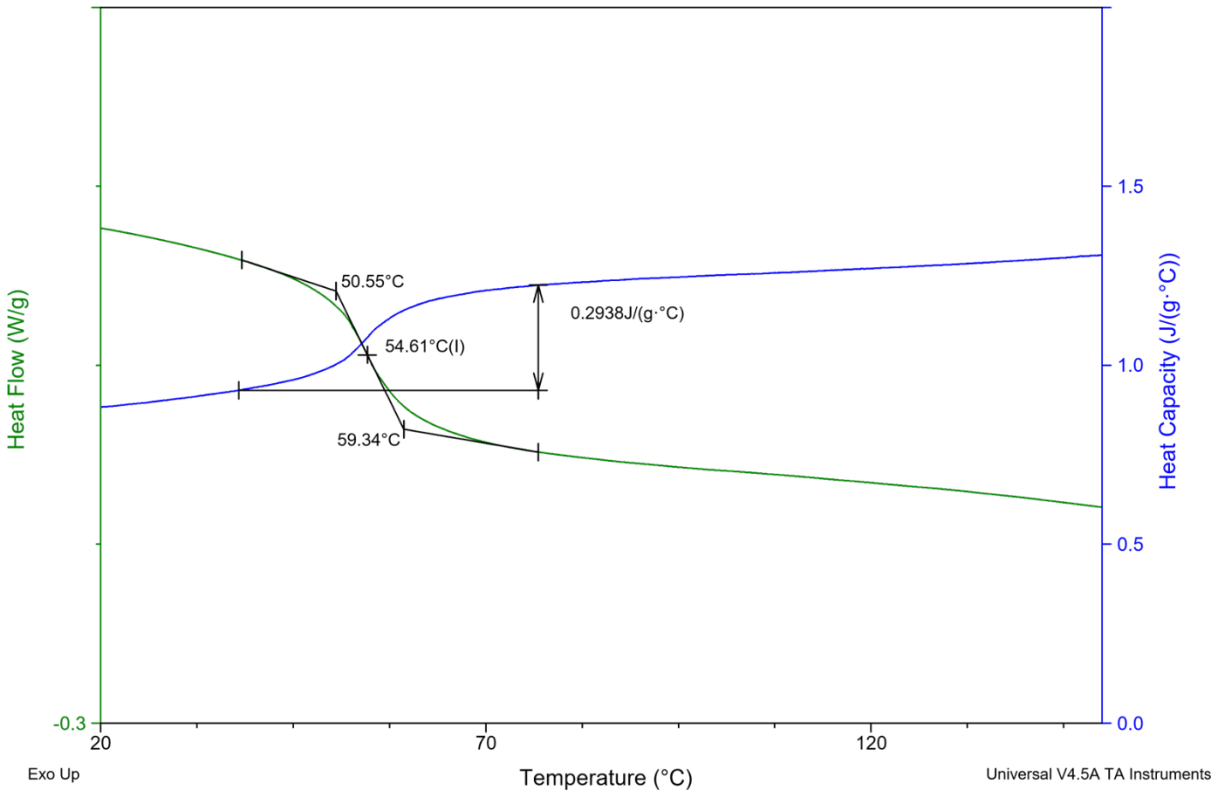

Figure S22. DSC traces of pTFBMA-Benzyl mercaptan (Table S3, entry 2)

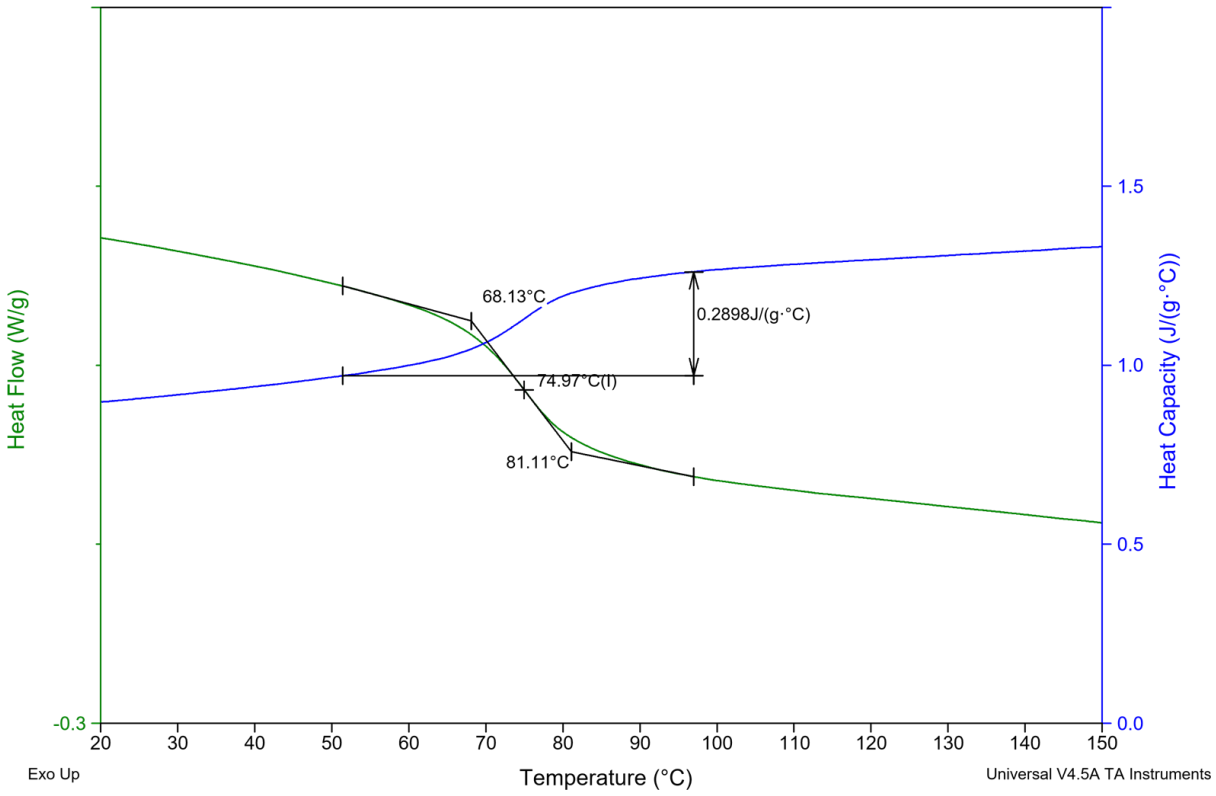

Figure S23. DSC traces of pTFBMA-4-Isopropylbenzenethiol (Table S3, entry 3)

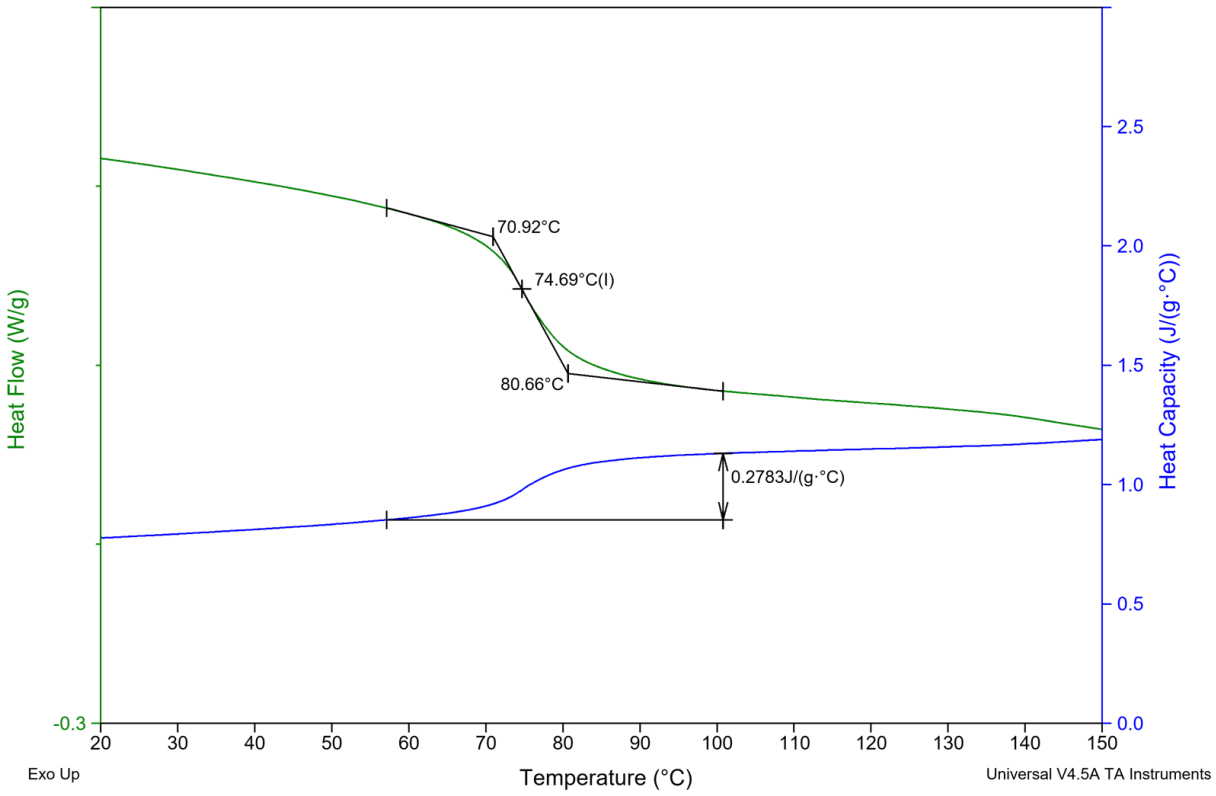

Figure S24. DSC traces of pTFBMA-Benzenethiol (Table S3, entry 4)

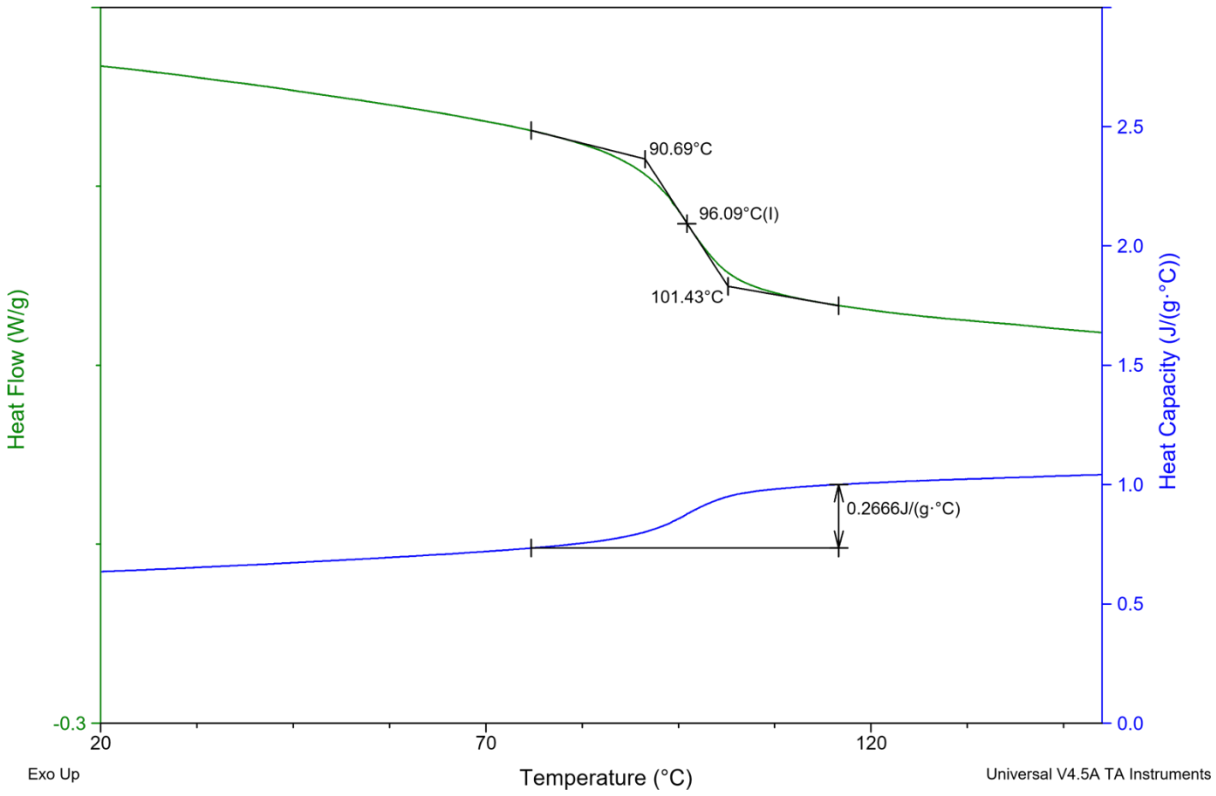

Figure S25. DSC traces of pTFBMA-4-tert-Butylbenzenethiol (Table S3, entry 5)

3.4.Calculation of the glass transition temperature of the cores of PISA particles

Table S4. The T_g of copolymers can be estimated by the Fox equation and Gordon-Taylor (or Couchman-Karasz derivation) equations.

					Fox Equation			Gordon–Taylor Equation	
	Monomer Molar Mass (g/mol)	Molar Fraction (pTFBMA -thiol)	Weight Fraction (pTFBMA -thiol)	Measured T_g homopolymer (K)	$T_{g,calc}$ Copolymer Core (K)	$T_{g,calc}$ Copolymer Core (°C)	Heat Capacity Change ΔCp (mJ/K)	$T_{g,calc}$ Copolymer Core (K)	$T_{g,calc}$ Copolymer Core (°C)
poly(PFBMA)	266.17	0	0	338.2	-	-	0.78	-	-
reacted with butanethiol	336.34	0.64	0.69	286.5	300.7	27.5	1.69	295.4	22.2
reacted with benzyl mercaptan	370.36	0.98	0.99	323.7	323.9	50.8	1.38	323.8	50.7
reacted with 4-isopropylbenzenethiol)	398.42	0.42	0.52	341.3	339.8	66.6	1.10	340.0	66.9
reacted with benzenethiol)	356.33	0.48	0.55	344.1	341.4	68.2	1.34	342.2	69.0
reacted with 4-*tert*-Butylbenzenethiol)	412.44	0.38	0.49	363.8	350.2	77.0	1.17	353.2	80.1

If *1* is the thiol-modified PPFBMA and *2* is unreactied PPFBMA,

- Molar Fractions

Molar fractions were determined by ^{1}H NMR

Molar fraction can be expressed as $x_1 = \frac{n_1}{n_1+n_2}$ for 1 and $x_2 = \frac{n_2}{n_1+n_2}$ for 2.

- Weight Fractions

Mass (or weight) fraction (w) of 1 is $w_1 = \frac{m_1}{m_1+m_2} = \frac{x_1 M_1}{x_1 M_1+x_2 M_2}$ and of 2 is $w_2 = \frac{x_2 M_2}{x_1 M_1+x_2 M_2}$

Where M_1 and M_2 are, respectively, the molar mass of 1 and 2

- Fox equation

$$\frac{1}{T_{g,mix}} \approx \frac{w_1}{T_{g,1}} + \frac{w_2}{T_{g,2}}$$

- Gordon-Taylor equation [7]

$$T_{g,mix} \approx \frac{w_1 \Delta C_{p,1} T_{g,1} + w_2 \Delta C_{p,2} T_{g,2}}{w_1 \Delta C_{p,1} + w_2 \Delta C_{p,2}}$$

In the main manuscript, values calculated by the Gordon-Taylor equation are reported.

4. References

1 J. M. Noy, A. K. Friedrich, K. Batten, M. N. Bhebhe, N. Busatto, R. R. Batchelor, A. Kristanti, Y. Pei and P. J. Roth, *Macromolecules*, 2017, **50**, 7028–7040.

2 N. Busatto, V. Stolojan, M. Shaw, J. L. Keddie and P. J. Roth, *Macromol. Rapid Commun.*, 2019, **40**, 1800346.

3 E. R. Jones, M. Semsarilar, A. Blanazs and S. P. Armes, *Macromolecules*, 2012, **45**, 5091–5098.

4 E. R. Jones, M. Semsarilar, P. Wyman, M. Boerakker and S. P. Armes, *Polym. Chem.*, 2016, **7**, 851–859.

5 M. J. Derry, L. A. Fielding and S. P. Armes, *Polym. Chem.*, 2015, **6**, 3054–3062.

6 A. Blanazs, J. Madsen, G. Battaglia, A. J. Ryan and S. P. Armes, *J. Am. Chem. Soc.*, 2011, **133**, 16581–16587.

7 P. R. Couchman and F. E. Karasz, *Macromolecules*, 1978, **11**, 117–119.